# Modeling and Analysis of a Heat Pump Clothes Dryer with Thermal Energy Storage

Xiaoli LIU[1], Cheng-Min YANG[1], Pengtao WANG[1], Kashif NAWAZ[1]*, Christopher HARTNETT[2], Arun RAJENDRAN[2], Troy SEAY[1]

[1]Multifunctional Equipment Integration Group, Oak Ridge National Laboratory,
Oak Ridge, Tennessee, United States of America,
xiaoli@ornl.gov; yangc1@ornl.gov; wangp@ornl.gov; nawazk@ornl.gov; seaytw@ornl.gov

[2]Whirlpool Corporation,
United States of America,
christopher_a_hartnett@whirlpool.com; arun_rajendran@whirlpool.com

* Corresponding Author

## ABSTRACT

Clothes drying is an energy-intensive process that causes significant electricity consumption and carbon emissions in the US. Approximately 83% of households in the US own a tumble clothes dryer at home and 80% of dryers are electrical resistance dryers with low energy efficiency. Heat pump technology makes it possible for highly efficient and clean drying. Additionally, the ventless design of heat pump clothes dryers (HPCD) provides more installation flexibility. The operation of HPCD involves three primary mediums: wet clothes, a closed air loop, and a refrigerant circuit. The evaporator is for dehumidifying the wet air and the condenser is for re-heating the dry air. One of the critical technological barriers to HPCD market penetration is its long drying time, primarily due to the relatively low discharging temperature and the slow response during the initial warm-up period. In this study, thermal energy storage (TES) technology was adopted to address this challenge by providing pre-heating of air prior to the condenser to increase the operating temperature of the process air. The heat pump can charge the phase change material (PCM) in the TES device with heating energy during clothes washing and the PCM will discharge the stored heat to facilitate air heating during clothes drying. To analyze the optimal design and potential for energy saving and drying time reduction, a mathematical model of the HPCD system was developed. The HPCD is a highly dynamic system with coupled heat and mass transfer and heat pumping cycle. This paper provides solutions to simulate the transient behavior of the system while maintaining low computational cost. The modeling result indicated that the new system had reduced energy consumption compared to electrical resistance dryers and a faster drying time compared to HPCDs. The study provided significant insights into improving building flexibility with TES and smart appliances.

## 1. INTRODUCTION

Clothes dryers have become an essential household appliance in modern society and have witnessed steady growth in recent years. In 2020, nearly 83% of US households (equal to 102.32 million) had a clothes dryer at home (EIA, 2020). Though the penetration of clothes dryers in the U.S. remains high, around 29% of the residential dryers are more than 10 years old (EIA, 2020). Clothes drying in modern society is an energy and carbon-intensive process. In the US, clothes dryers consumed about 64 billion kWh of electricity in 2021, accounting for 4.2% of the total electricity use in residential buildings (EIA, 2020). The laundry activities, mostly the clothes drying, lead to an equivalent carbon emission of around 32.9 MMmt $CO_2$, sharing 3.5% of total residential emissions (*Annual Energy Outlook*, 2023).

Commercially available clothes dryers include four primary configurations as displayed in Figure 1: (1) vented electric/gas dryer, (2) ventless electric dryer (or condensing dryer), (3) heat pump dryer, and (4) hybrid heat pump dryer. In the US, thermal drying systems dominate the residential clothes dryers with over 80% of them being

vented electric resistance dryers and less than 20% of them being gas-fired dryers (EPA, 2011). To advance energy efficiency in clothes drying, the first electric heat pump clothes dryer (HPCD) was developed in Europe by Electrolux in 1997 (Meyers et al., 2010). In 2014, the HPCD was first available in the US market and ENERGY STAR started to include dryers in the rating program. HPCD can reduce energy use by at least 28% compared to standard dryers (*Heat Pump Dryer | ENERGY STAR*, n.d.). Today, most HPCDs use R-134a as the refrigerant and there are about three products using the low global warming potential (GWP) refrigerant R-290. As shown in Figure 1, the HPCD uses the evaporator to dehumidify the process air and uses the condenser to heat the air to be supplied to the drum. Using an evaporator to condense excess water vapor in the process air allows the HPCD to be operated in a ventless configuration where no fresh air is introduced to the system and no exhaust air is released. The ventless HPCD offers great installation flexibility due to two primary factors. Firstly, unlike vented dryers, the HPCD doesn't require connection to outlet air ducts and provides more flexibility for installation. Second, the exhaust moist air in a vented clothes dryer is a major waste heat; recovering this waste heat by heat pump technology contributes to higher energy efficiency. Third, the power consumption of HPCD is significantly lower compared to electric resistance dryers, making it compatible with 120 V systems and reducing the necessity for electric circuit upgrades.

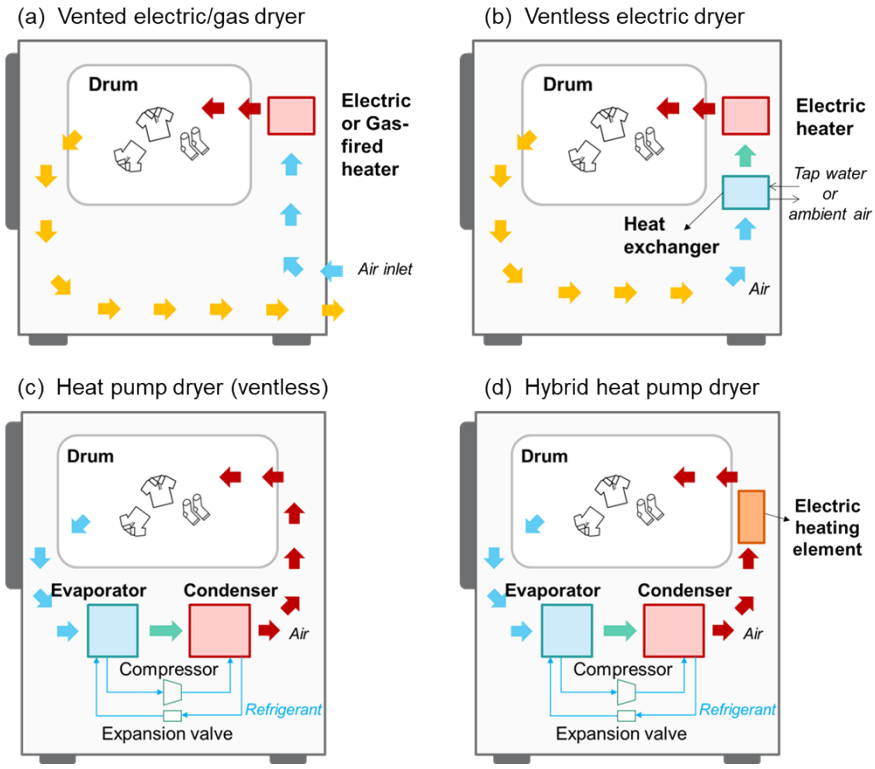


**Figure 1:** System configurations of clothes dryers: (a) vented electric resistance dryer, (b) ventless electric resistance dryer, (c) ventless heat pump dryer, and (d) ventless hybrid heat pump dryer.

Research on HPCDs has been continuously increasing in recent years. Huang et al., (2020) compared the performance of three domestic clothes dryers experimentally, including HPCD, electric resistance type, and gas-fired type. The results showed that HPCD performed the best energy-related metrics whereas gas-fired dryers had the highest moisture extraction rate (MER). Till now, the HPCD has gained a small market share due to its high initial cost and performance challenges. As shown in Figure 2, the main technological challenges of the HPCD include the longer drying time and smaller capacity (due to the size of heat pump units). The lower operating air temperature leads to a low MER. Additionally, the heat pump unit takes time to warm up the system at the initial drying phase. Therefore, HPCD tends to have a longer drying time. A commercially available hybrid dryer (Figure 1(d)) utilizing the electric resistance element to boost the air temperature at the initial drying period helps increase the overall drying speed while maintaining a certain level of energy efficiency. However, this hybrid HPCD design requires large power draw and is not compatible with 120 V systems.

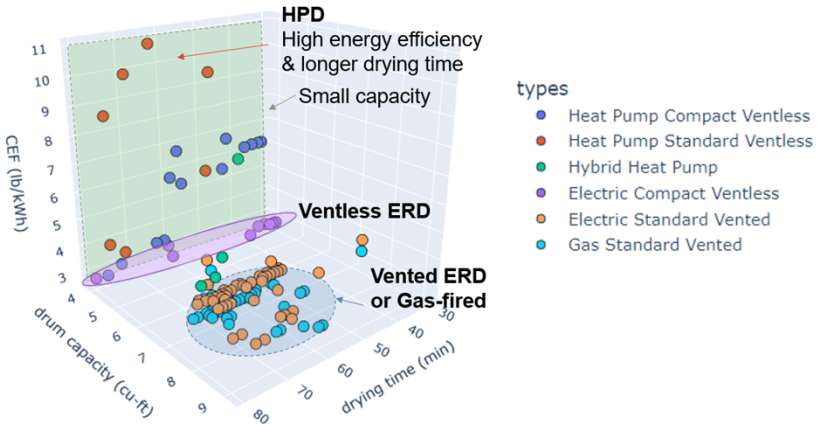


**Figure 2:** A diagram comparing CEF, drum capacity, and drying time of different ENERGY STAR® clothes dryers.

In this study, we proposed an alternative solution that uses thermal energy storage (TES) technology to address the drying time challenge faced by HPCDs while maintaining a high level of efficiency and building flexibility. The TES technology has gained significant attention in recent years, particularly latent heat thermal energy storage (LHTES). LHTES involves storing thermal energy using phase change materials (PCM) that can store and release large amounts of energy during phase transitions (e.g., gas to liquid, solid to gas, solid to solid, or solid to liquid). PCMs have a high energy density and near-constant temperature during phase changes, making them beneficial for thermal buffering, load shifting, peak shaving, and footprint reduction in energy storage (Freeman et al., 2023). Among all types of TES materials, solid-liquid PCMs offer the most compelling energy density and find widespread use in building applications (Shah et al., 2022).

Integrating the TES device into a combined washer and HPCD enables a fast and energy-efficient operation. As illustrated in Figure 3, the proposed system has a dual evaporator and a TES device, in addition to the conventional HPCD configuration. The combined washer and dryer is an all-in-one unit, starting from washing, the heat pump system runs to charge the TES device and the refrigerant bypasses the primary evaporator and flows through the evaporator outside the cabinet to source heat from the ambient (Figure 3a). On the TES side, hot refrigerant vapor dissipates heat into the PCM when flowing through the TES device and becomes hot fluid. No internal air flow occurs in this mode. When the washing is done, the system switches to the drying mode and the heat pump runs with the primary evaporator and condenser to process the circulating air. The TES device works as an air-to-PCM heat exchanger to preheat the process air prior to the condenser. Because of the preheating, the discharging temperature of the heat pump cycle increases, allowing the system to warm up quickly. When the TES is fully discharged, the system runs as a conventional HPCD.

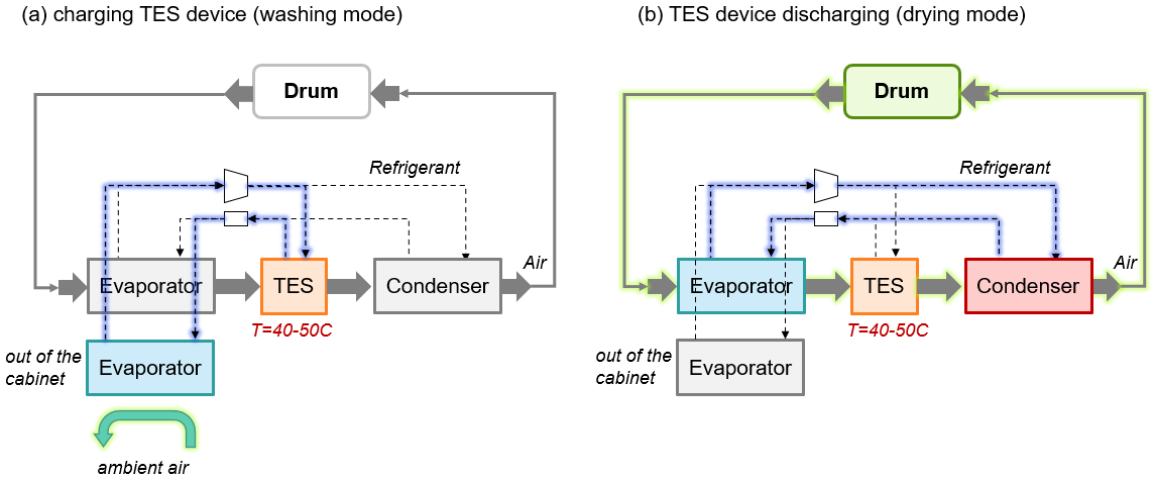


**Figure 3:** System diagram of an HPCD integrated with TES for air pre-heating operating in two modes.

The design of TES device for HPCD is critical to the system's successful operation. We proposed and developed a three-medium heat exchanger utilizing PCM to advance the performance of HPCD. As displayed in Figure 4(a), the heat exchanger has a fin-tube configuration with inner refrigerant tubes and outer PCM tubes. The PCM is static inside the tube and should be well-sealed. The inertial fins are used to enhance the heat transfer from the refrigerant to PCM during the charging mode. This innovative design allows the heat exchanging and storage to be operating in one device, avoiding the secondary loop for thermal storage and associated fluid pump. In this way, the overall system could be more compact. As shown in Figure 4(b), sixteen elements are used for the complete heat exchanger design and placed into a staggered configuration to enhance the turbulence of air flow.

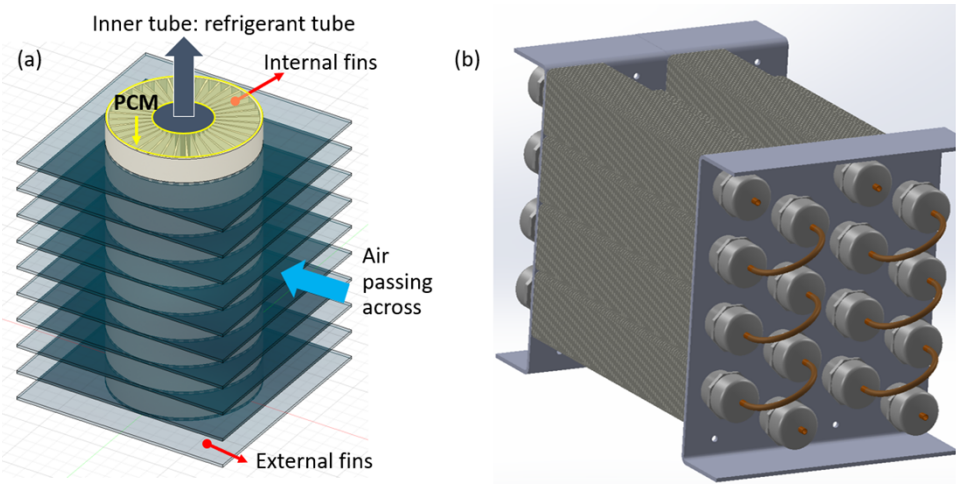


**Figure 4:** The 3D drawing of the three-medium PCM HX for HPCD integration.

To prove the concept of HPCD with TES, we developed a quasi-steady-state model to numerically investigate the system's thermodynamic performance. The method and result presented contribute to the direct integration of latent TES into air conditioning systems, the application of TES in smart appliances, and TES design and control.

## 2. METHODOLOGY

As displayed in Figure 5, the HPCD system consists of two circuits: refrigerant vapor compression cycle and closed air loop. The vapor compression cycle contains four primary components, including the air-to-refrigerant evaporator, air-to-refrigerant condenser, expansion valve, and compressor. Most HPCDs have a ventless design where the process air forms a closed air loop within the dryer cabinet. The closed-air loop contains the tumbler drum, filter (or lint screens), and blower.

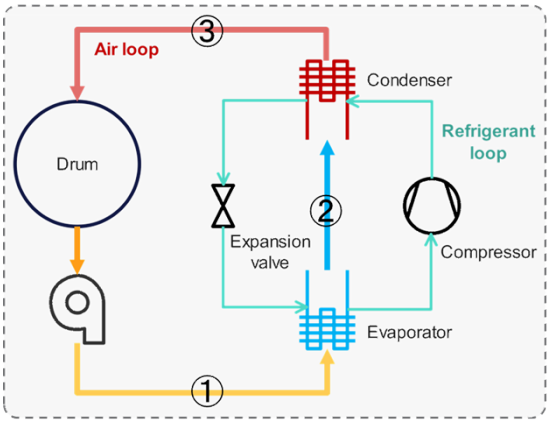


**Figure 5:** System diagram of a conventional HPCD (Zhang, 2015).

Due to the transient operation and coupled heat and mass transfer, the HPCD becomes a complex system. A full-dynamic model is computationally expensive and requires a large amount of experimental data to calibrate all component models. To simplify the system while maintaining good accuracy in predicting the variation of fabric status, a quasi-steady-state model was developed where the heat pump system reaches steady-state at each discrete time step (Shen et al., 2016). The drum model involved the heat and mass balance of dry air, water vapor, and wet clothes. A first principle-based thermodynamic model was established to capture the transient behavior in the drum.

### 2.1 Vapor Compression Cycle Simulation

The AHRI 10-coefficient compressor map was used to determine the performance of a single-speed compressor (*AHRI Standard 540*, n.d.). The 10-coefficient polynomial provided by the manufacturer computes the refrigerant mass flow rate and compressor power consumption. The condenser and evaporator are air-cooled fin-and-tube heat exchangers. The overall heat transfer rate was evaluated by a lumped model, where a constant condensing or evaporating temperature was used and obtained at the heat exchanger's inlet pressure. The ε-NTU method determines the global conductance and heat transfer effectiveness relations. The conductance was obtained from the heat exchanger data. The throttling process is assumed to be adiabatic and isenthalpic.

### 2.2 Air Circuit Simulation

The air in the closed loop undergoes three processes – (1) dehumidification and cooling, (2) heating, and (3) humidification and cooling. The process air was dehumidified when it passed across the evaporator. Then the process air was heated as it passed across the condenser. The behavior of air coupled with the varying status of the refrigerant at the heat exchangers. A lumped model was used to predict the cooling and heating energy applied to the process air. Inside the drum, the air humidification and cooling are a more dynamic process. The governing equations are generated based on the conservation of heat and mass (Cao et al., 2021; Lee et al., 2019; Yadav & Moon, 2008).

### 2.3 TES Simulation

The TES device used in the system is a three-medium heat exchanger. The PCM absorbs heat from the refrigerant vapor during the charging process and releases heat to the air during the discharging process. The TES device was modeled by a one-dimensional (1-D) heat conduction model in a cylindrical coordinate and solved by a finite difference method. The heat transfer at the PCM boundary to the refrigerant or air was described by the product of the effective heat transfer coefficient, heat transfer area, and temperature difference between the PCM and boundary fluid. The latent heat storage capacity and the PCM state (liquid fraction) were modeled by the enthalpy method, where the PCM temperature is a function of enthalpy (Fortunato et al., 2012; Trp et al., 2004).

### 2.4 Solution

A quasi-steady-state solution was adopted in this study to solve the HPCD system model. At the moment i, the steady-state heat pump system model determines the refrigerant status and air status at compartment outlets based on the boundary conditions (i.e., air inlet temperature and humidity at the evaporator side). It is worth noting that the computed air condition at the evaporator outlet becomes the inlet condition at the condenser side. CVODE solver was used to determine the solution for the heat pump system governed by physical-based equations. Then, the condenser air outlet condition at the moment i, obtained from the heat pump model, becomes the inlet condition of the drum model at the air loop. The transient energy and mass balances were performed to compute the air status at the drum outlet at the moment i, which becomes the evaporator air inlet condition at the next time step (i.e., moment i+1). The governing equations of the drum model form a set of first-order partial differential equations, solved by the explicit method. Finally, the status variations of air, clothes, and refrigerant are numerically computed.

### 2.5 Performance Metrics

The remaining moisture content (RMC) in the clothes is defined as the mass ratio of water ($m_w$) to the bone-dry mass of the clothes ($m_{BD}$). In this paper, the drying time is defined as the time spent drying clothes from the initial RMC of 57.5% to the RMC of 3.5%.

$$RMC = \frac{m_w}{m_{clo}} \tag{1}$$

The combined energy factor (CEF) is a critical performance metric used in ENERGY STAR, defined as the bone-dry mass of clothes to the combined total energy consumption per cycle, expressed in lb./kWh.

$$CEF = \frac{m_{clo}}{E_{CC}} \tag{2}$$

where $E_{CC}$ is the combined total energy consumption calculated by the sum of electricity in drying operation ($E_{ce}$) and in standby and off modes. The CEF should be obtained from the experimental data. In this study, we ignored the energy consumed in standby and off modes and followed Eq. 2 to compute the theoretical CEF for performance comparison on various dryer configurations.

## 3. Model Validation and Calibration

### 3.1 Fabric Drying Model Validation

The transient drum model was validated by comparing the simulation result of a vented compact electric resistance clothes dryer to the experimental data published in the literature from Yadav (Yadav & Moon, 2008). The dryer was manufactured by Fisher & Paykel with a model number ED56. Figure 6 compares the simulation results and experimental data, as well as the simulation results from other two literatures. Good agreements can be found in figures regarding air relative humidity at the drum outlet and RMC. A large discrepancy is shown in the air outlet temperature. One primary reason could be the ignorance of the specific heat of dryer components. Another primary reason might be the ignorance of air leakage. Cao pointed out that two other reasons were from the calculation of activity factor and unsatisfied air equilibrium (Cao et al., 2021).

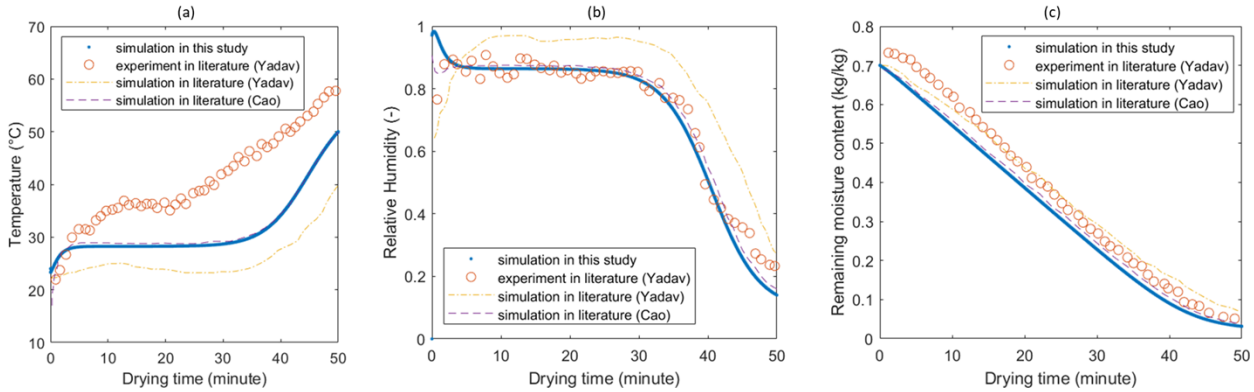


**Figure 6:** Drying performances validation of a compact electric resistance clothes dryer.

### 3.2 HPCD Model Calibration

The HPCD model was then constructed by a verified fabric-drying model described in Sections 2.2 and 3.1 and a calibrated heat pump model in Section 2.1. The model was parameterized using the data provided by the manufacturer as shown in Table 1 and the calibration was carried out by the standard test results of evaporator, condenser, and the whole HPCD unit. This modeling method of HPCD was referred to a rational-based model (Lee et al., 2019).

**Table 1:** Parameters used in the HPCD model.

| Components | Parameters | Values |
|---|---|---|
| Condenser | Condensing pressure | 20 bars |
| | Condensing temperature | 65 ºC |
| | Subcooling degree | 20 ºC |
| Evaporator | Evaporating pressure | 7 bars |
| | Evaporating temperature | 26 ºC |
| | Superheating degree | 15 ºC |
| Drum | Air flow rate | 0.02 kg/s |

| Dryer | CEF | 5.2 lb./kWh |
|---|---|---|

## 4. Simulation Results

### 4.2 Drying Performance of a Standard HPCD

Figure 7 displays performance curves of a standard HPCD. These curves show three distinct drying phases: initial, constant, and falling phases. In the initial phase, the heat pump's evaporating and condensing temperatures start low but progressively increase over time. Consequently, both air and clothes temperatures gradually rise and the rate of evaporation at the fabric surface remains low. In this phase, most of the heat supplied to the process air is utilized for enhancing the sensible heat of the air and fabric. As the HPCD operates within a closed air loop, with an increasing evaporator air inlet temperature, the suction and discharge temperatures of the refrigerant, along with the drum air inlet temperature, continue to increase, leading to the highest rate of evaporation. Subsequently, the system enters the constant phase, during which the temperatures of the air, clothes, and refrigerant remain relatively stable. In the constant phase, due to the balance between the evaporator's cooling capacity, the condenser's heating capacity, and heat and mass transfer within the drum, most heat supplied to the drum air is used for removing the latent load, that is evaporating the water vapor from clothes. However, due to the dynamics of the HPCD system, this constant phase is not as flat as the vented one (Figure 6). Next, the system moves to the falling phase. Prior to the typical falling phase, the HPCD experiences a pre-falling phase where the condensing and evaporating temperatures drop for a short period (Figure 8), which occurs near a drying time of 40-50 min. The heat pump's evaporating temperature drops because the air humidity at the drum outlet drops due to the reduced rate of evaporation and therefore the sensible load ratio at the evaporator increases. With a lower evaporating temperature, the condensing temperature also reduces. However, in the later part of the falling phase, the heat pump's condensing and evaporating temperatures begin to rise dramatically. This is because the rate of evaporation becomes extremely low and the heat from the condenser largely increases the air and clothes temperature. At this moment, the sensible heat ratio is close to one and the dehumidification cannot be proceeded. This clothes-drying process takes 70 min to dry a total mass of 3.83 kg of clothes from the initial RMC of 57.5% to the final RMC of 3.5%. The CEF calculated using Eq.2 is around 5.2 lb./kWh.

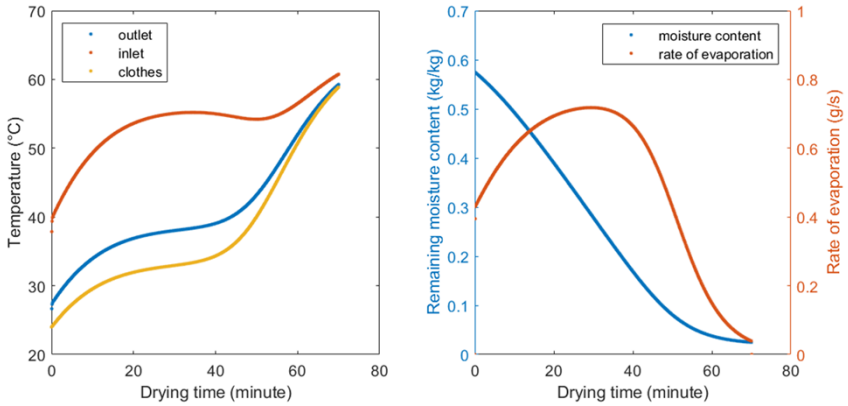


**Figure 7:** Drying performance of a standard ventless HPCD.

The variation of refrigerant status in the heat pump cycle is presented in Figure 8. As we explained above, the p-h diagram of the cycle gradually moves upwards with time, due to the change in vapor evaporation rate of wet clothes, evaporating temperature, and condensing temperature.

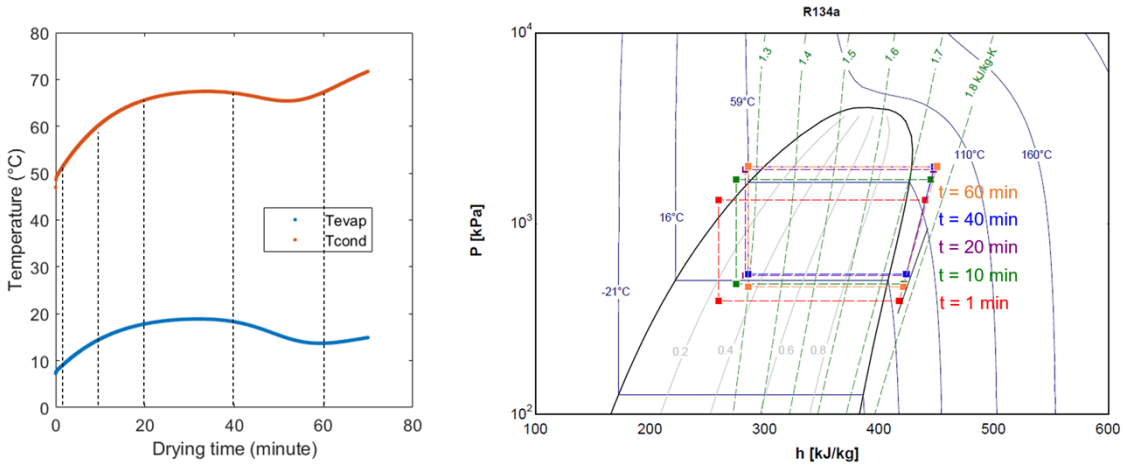


**Figure 8:** Refrigeration status variation in the heat pump cycle.

### 4.3 Drying Performance of a Standard HPCD with TES

This section investigated two scenarios: one where TES operated throughout the entire drying period, and the other where TES was only operational during the initial phase. In the first case, the drying time of the HPCD-TES system was significantly reduced to 52 min. A reduction of 25.7% in the drying time was observed, compared to the standard HPCD system. As shown in Figure 9, the rate of evaporation of the HPCD-TES system is higher and steep, with a maximum rate of 1 g/s. This is primarily due to the increased discharging temperature of the refrigerant and the air temperature at the drum inlet. A maximum temperature of 70 °C can be reached at the drum inlet. However, the increase in discharge temperature also leads to the COP decrease. The efficiency of TES charging and discharging plays a critical role in determining the overall energy efficiency of the system. As a result, we observed a decrease in the CEF. To improve the system's efficiency, the second case was studied by discharging the TES for the first 20 min. As a result, the drying time of 56 min and a CEF of around 5.0 lbs/kWh can be reached. The CEF is 27% higher than that of the electric resistance type of clothes dryers.

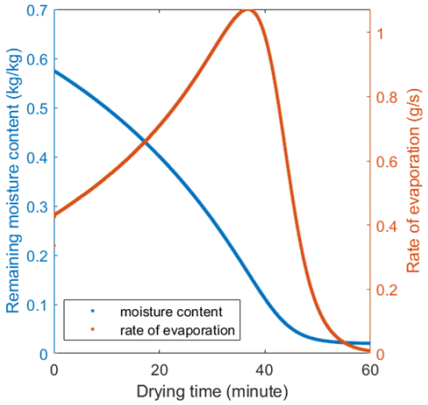


**Figure 9:** The drying curve and rate of evaporation of a HPCD with TES.

## 5. Limitations and Challenges

The model of HPCD with TES developed in this paper adopted a quasi-steady-state approach to achieve higher computational efficiency while maintaining the ability to capture the dynamic and transient behavior of the drying process. This study contributes to a deeper understanding of the HPCD's mechanism from a first-principles perspective. However, the HPCD with TES is a highly complex thermodynamic system and its complexity mainly lands in (1) the coupled air inlet/outlet states on the evaporating and condensing sides, (2) two coupled closed loops of air and refrigerant, (3) the coupled heat and mass transfer problem between air and clothes inside the drum, and (4) the dynamic air-side behavior throughout the whole drying process. Therefore, certain assumptions and

simplifications are necessary to ensure the model's robustness. However, there exist limitations in this model that require further improvement, as described below:

(1) The system model underestimates the thermal inertia of both the heat pump system and the drum.
(2) The current stage of the system model does not incorporate the process control of the dryer.
(3) The TES model ignores the impact of volume changes and subcooling in PCM during phase transition.
(4) The TES model ignores the effects of natural convection and gravity on PCM.

## 6. Conclusions

In this effort, we proposed a novel HPCD system integrating TES for higher energy efficiency and faster operation. A first-principle-based numerical model of the system was developed and solved by a quasi-steady-state approach. The model predicts the dynamic behavior of the HPCD such as air and refrigerant temperatures, RMC, etc. Modeling results indicate that the HPCD with TES system can reduce up to 25.7% of drying time. The energy efficiency of the new system highly depends on the capacity and efficiency of the TES device and its operation time. In addition, the use of TES in appliances facilitates building flexibility and smart building energy management, which provides an alternative solution for load shifting and power reduction in buildings.

## NOMENCLATURE

The nomenclature should be located at the end of the text using the following format:

| | | |
|---|---|---|
| CEF | combined energy factor | (lbs/kWh) |
| HPCD | heat pump clothes dryer | |
| MER | moisture extraction rate | (kg/hr) |
| RMC | remaining moisture content | (% or kg/kg) |
| TES | thermal energy storage | |

**Subscript**

| | |
|---|---|
| a | air |
| ai | air inlet |
| ao | air outlet |
| clo | clothes |
| comp | compressor |
| fan | fan |
| w | water |

## REFERENCES

*AHRI Standard 540*. (n.d.). Retrieved June 7, 2024, from https://www.ahrinet.org/system/files/2023-06/AHRI_Standard_540_%28I-P_and_SI%29_2020_Standard_for_Performance_Rating_of_Positive_Displacement_Refrigerant_Compressors_and_Compressor_Units.pdf

*Annual Energy Outlook*. (2023). https://www.eia.gov/outlooks/aeo/index.php

Cao, X., Zhang, J., Li, Z.-Y., Shao, L.-L., & Zhang, C.-L. (2021). Process simulation and analysis of a closed-loop heat pump clothes dryer. *Applied Thermal Engineering*, *199*, 117545. https://doi.org/10.1016/j.applthermaleng.2021.117545

EIA. (2020). *2020 Residential Energy Consumption Survey (RECS) Housing Characteristic Data*. https://www.eia.gov/outlooks/aeo/data/browser/#/?id=4-AEO2022&region=0-0&cases=ref2022&start=2020&end=2050&f=A&linechart=~ref2022-d011222a.29-4-AEO2022&ctype=linechart&sourcekey=0

EPA. (2011). *ENERGY STAR Market & Industry Scoping Report Residential Clothes Dryers* (p. 18). https://www.energystar.gov/sites/default/files/asset/document/ENERGY_STAR_Scoping_Report_Residential_Clothes_Dryers.pdf

Fortunato, B., Camporeale, S. M., Torresi, M., & Albano, M. (2012). Simple Mathematical Model of a Thermal Storage with PCM. *AASRI Procedia*, *2*, 241–248. https://doi.org/10.1016/j.aasri.2012.09.041

Freeman, T. B., Foster, K. E. O., Troxler, C. J., Irvin, C. W., Aday, A., Boetcher, S. K. S., Mahvi, A., Smith, M. K., & Odukomaiya, A. (2023). Advanced Materials and Additive Manufacturing for Phase Change Thermal Energy Storage and Management: A Review. *Advanced Energy Materials*, *13*(24), 2204208. https://doi.org/10.1002/aenm.202204208

*Heat Pump Dryer | ENERGY STAR*. (n.d.). Retrieved April 29, 2024, from https://www.energystar.gov/products/clothes_dryers/heat-pump-dryer

Huang, X.-M., Xiong, L., Zheng, Y.-W., Liu, H.-Q., Xu, Y.-Z., & Li, Y.-C. (2020). Comparative investigation of performance of gas dryer and two other types of domestic clothes dryers. *International Journal of Low-Carbon Technologies*, *16*. https://doi.org/10.1093/ijlct/ctaa064

Lee, B.-H., Sian, R. A., & Wang, C.-C. (2019). A rationally based model applicable for heat pump tumble dryer. *Drying Technology*, *37*(6), 691–706. https://doi.org/10.1080/07373937.2018.1454940

Meyers, S., Franco, V. H., Lekov, A. B., Thompson, L., & Sturges, A. (2010). *Do Heat Pump Clothes Dryers Make Sense for the U.S. Market? | Energy Efficiency Standards*. https://ees.lbl.gov/publications/do-heat-pump-clothes-dryers-make

Shah, K. W., Ong, P. J., Chua, M. H., Toh, S. H. G., Lee, J. J. C., Soo, X. Y. D., Png, Z. M., Ji, R., Xu, J., & Zhu, Q. (2022). Application of phase change materials in building components and the use of nanotechnology for its improvement. *Energy and Buildings*, *262*, 112018. https://doi.org/10.1016/j.enbuild.2022.112018

Shen, B., Gluesenkamp, K., Bansal, P., & Beers, D. (2016). *Heat Pump Clothes Dryer Model Development*.

Trp, A., Lenic, K., & Franković, B. (2004). *A Study of Transient Phase-Change Heat Transfer During Charging and Discharging of the Latent Thermal Energy Storage Unit*. https://www.semanticscholar.org/paper/A-Study-of-Transient-Phase-Change-Heat-Transfer-and-Trp-Lenic/cb9593d1e0c557b330c6913f0b252c841acbd5e5

Yadav, V., & Moon, C. G. (2008). Fabric-drying process in domestic dryers. *Applied Energy*, *85*(2), 143–158. https://doi.org/10.1016/j.apenergy.2007.06.007

Zhang, Z. (2015). *Analysis of Heat Pump Clothes Dryer* [Thesis]. https://doi.org/10.13016/M27H1C

## ACKNOWLEDGEMENT

This study was funded by the US Department of Energy (DOE) Office of Energy Efficiency and Renewable Energy, Building Technologies Office (BTO). The authors would also like to thank the support from the technology manager of Building Electric Appliances, Devices, and Systems (BEADS), Dr. Wyatt Merrill. This manuscript has been authored by UT-Battelle, LLC, under contract DE-AC05-00OR22725 with the US Department of Energy (DOE). The US Government retains and the publisher, by accepting the article for publication, acknowledges that the US government retains a nonexclusive, paid-up, irrevocable, worldwide license to publish or reproduce the published form of this manuscript or allow others to do so, for the US government purposes. DOE will provide public access to these results of federally sponsored research in accordance with the DOE Public Access Plan (http://energy.gov/downloads/doe-public-access-plan).